ROYAL SOCIETY OPEN SCIENCE

rsos.royalsocietypublishing.org

Research

**Cite this article:** Ding H, Lv J, Wu H, Chai G, Liu A. 2018 Enhanced light-harvesting by plasmonic hollow gold nanospheres for photovoltaic performance. *R. Soc. open sci.* **5**: 171350.
http://dx.doi.org/10.1098/rsos.171350

Received: 19 September 2017
Accepted: 14 December 2017

**Subject Category:**
Chemistry

**Subject Areas:**
energy/nanotechnology

**Keywords:**
hollow gold nanospheres, $TiO_2$ nanorod, surface plasmon resonance, photochemical performance, solar cell

**Authors for correspondence:**
Huaping Wu
e-mail: wuhuaping@gmail.com
Aiping Liu
e-mail: liuaiping1979@gmail.com

This article has been edited by the Royal Society of Chemistry, including the commissioning, peer review process and editorial aspects up to the point of acceptance.

THE ROYAL SOCIETY PUBLISHING

# Enhanced light-harvesting by plasmonic hollow gold nanospheres for photovoltaic performance

Hao Ding[1], Jindian Lv[2], Huaping Wu[1], Guozhong Chai[1] and Aiping Liu[2,3]

[1]Key Laboratory of E&M, Ministry of Education, Zhejiang University of Technology, Hangzhou 310014, People's Republic of China
[2]Center for Optoelectronics Materials and Devices, Zhejiang Sci-Tech University, Hangzhou 310018, People's Republic of China
[3]State Key Laboratory of Nonlinear Mechanics, Institute of Mechanics, Chinese Academy of Sciences, Beijing 100190, People's Republic of China

HD, 0000-0001-8281-6983

A 'sandwich'-structured $TiO_2$NR/HGN/CdS photoanode was successfully fabricated by the electrophoretic deposition of hollow gold nanospheres (HGNs) on the surface of $TiO_2$ nanorods (NRs). The HGNs presented a wide surface plasmon resonance character in the visible region from 540 to 630 nm, and further acted as the scatter elements and light energy 'antennas' to trap the local-field light near the $TiO_2$NR/CdS layer, resulting in the increase of the light harvesting. An outstanding enhancement in the photochemical behaviour of $TiO_2$NR/HGN/CdS photoanodes was attained by the contribution of HGNs in increasing the light absorption and the number of electron-hole pairs of photosensitive semiconductors. The optimized photochemical performance of $TiO_2$NR/HGN/CdS photoanodes by using plasmonic HGNs demonstrated their potential application in energy conversion devices.

## 1. Introduction

Recently, quantum dot-sensitized solar cells (QDSSCs) have attracted increasing interest and are considered as a potential alternative to silicon-based photovoltaic devices [1–3]. Titanium dioxide ($TiO_2$) with a wide-band gap (approx. 3.2 eV) is the most commonly used photoanode material in solar cells, which absorbs only ultraviolent light [4–6]. Generally, the light harvesting of QDSSCs is mainly determined by the quantum dot (QD) sensitizers, such as CdS [7–9], CdSe [10–12], CdTe [12] and

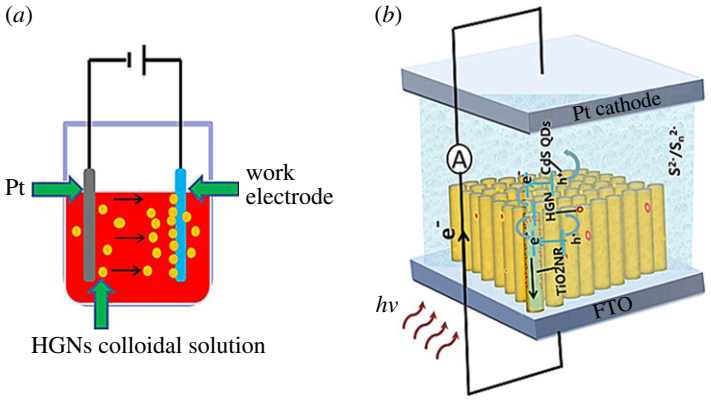


**Figure 1.** (*a*) Schematic of surface decoration strategy of $TiO_2$ nanorods electrodes based on electrophoretic deposition in the HGNs colloidal solution. The DC voltage was 35 V. (*b*) Schematic of separation and transfer of electron-hole pairs in CdS QD-sensitized $TiO_2$ solar cell with plasmonic HGNs.

PbS [13]. Narrow-bandgap QDs have high absorption cross section and absorb light in the visible to infrared (IR) range, which can be combined with wide-bandgap $TiO_2$ semiconductors to form a heterostructure and allow excellent charge transport [14–22].

In the past decades, considerable efforts to augment photovoltaic performance in QDSSCs by perfecting the counter electrode [23], electrolytes [24] and sensitizers [7–13] have been implemented. Noble metal nanoparticles (NPs), especially Au and Ag nanocrystals, have been given significant attention for their ability to couple incident photons in the visible to near IR region through the creation of surface plasmon resonances (SPRs) [25,26]. Plasmonic nanostructures can act as subwavelength scattering elements to fold light into a thin absorber, and also be used antennas to concentrate light energy surrounding them, which finally act as the electron sink for facilitating charge separation [27]. The plasmonic properties can be controlled by the type of the metal, size, shape, surrounding dielectric medium, distance between neighbouring objects and configuration of their ensemble [28–30]. For instance, Zhang *et al*. decorated CdSe-$TiO_2$ photoanode with Au NPs and found that the photocurrent increased to 85% and the photoconversion efficiency increased to 167% due to the electron sink of Au NPs [31]. Bardhan *et al*. demonstrated enhanced light harvesting in DSSCs with silica-coated Au nanocubes, resulting in a power conversion efficiency of 7.8% [32]. We also clarified the enhanced photovoltaic performance of CdS- or CdSe-sensitized photoanodes with plasmonic Au NPs as the efficient light scattering elements to couple and trap the sunlight [33,34].

Compared with the solid Au NPs, the hollow gold nanoparticles (HGNs) have stronger plasmon resonance and wider plasmonic tuning range [35,36]. However, as far as we know, there is no investigation of photovoltaic performance of DSSCs by employing HGNs as light scattering centres. In this paper, we introduce the HGNs into the $TiO_2$NR (nanorod) structure by a facile electrophoretic technology (figure 1*a*). The CdS sensitizer was deposited on the $TiO_2$NR/HGN surface by the successive ionic layer adsorption and reaction (SILAR) to construct the 'sandwich'-structured photoanodes (figure 1*b*). The physico-chemical properties of $TiO_2$NR/HGN/CdS photoanodes and their photovoltaic performances had been systematically studied, which would enable us to better understand SPR behaviour of HGNs in a photovoltaic material with adjustable light absorption and photovoltaic response.

# 2. Material and methods

## 2.1. Materials and reagents

FTO-coated glass (F : $SnO_2$, resistivity of 14Ω/square and thickness of 300 nm, Nippon Sheet Glass, Japan) was used as transparent conducting oxide substrate. Chloroauric acid ($HAuCl_4{\cdot}3H_2O$, 99.99%), sodium borohydride ($NaBH_4$), cadmium nitrate ($Cd(NO_3)_2$), sodium sulfide ($Na_2S$), sodium sulfite ($Na_2SO_3$) and titanium butoxide ($Ti(OCH_2CH_2CH_2CH_3)_4$, 99%) were purchased from Sigma-Aldrich Co. Trihydrate sodium citrate (TCD, $C_6H_5O_3N{\cdot}2H_2O$, purity 99%), cobalt chloride hexahydrate

($CoCl_2{\cdot}6H_2O$), hydrochloric acid (HCl, 36%), ethanol ($C_2H_6O$), methanol ($CH_4O$) and acetone ($C_3H_6O$) were supplied from Eagle Chemical Reagent Co. Ltd. All chemicals were of analytical grade and used as received. All aqueous solutions were prepared using deionized (D.I.) water with a resistivity of 18.2 MΩ cm prepared by Millipore Q purification system.

## 2.2. Preparation of citrate-stabilized hollow gold nanospheres

The citrate-stabilized HGNs are fabricated by using Co NPs as sacrificial templates with starting material of $HAuCl_4$ [37,38], as reported by Zhang *et al.* [39]. In brief, 75 ml of D.I. water was firstly placed into a three-necked Erlenmeyer bulb with 0.1 mol $l^{-1}$ TCD in a 35°C water bath, and the solution was deoxygenated by ultrapure argon. After 30 min, 100 µl of $CoCl_2$ (0.4 mol $l^{-1}$) was added into the flask under vigorous magnetic stirring (2500 r.p.m.), and a certain amount of fresh $NaBH_4$ (1 mol $l^{-1}$) was added into the mixture solution. The colour of solution was changed from pale pink to brown within tens of seconds, indicating the reduction of $Co^{2+}$ to cobalt NPs. After the hydrolysis reaction of $NaBH_4$ was finished, 30 ml Co NP colloidal solution was transferred to aqueous solution of $HAuCl_4$ (0.6 mmol $l^{-1}$, 10 ml) under continuous stirring. Finally, the as-prepared HGNs solution was centrifuged twice and re-dispersed into D.I. water. The solid gold nanoparticles (SGNs) used as a reference were synthesized by the classic Frens' method [35].

## 2.3. Preparation of photoanodes for photovoltaic cells

The FTO glass substrates (10 mm × 20 mm) were cleaned ultrasonically with acetone, ethanol and D.I. water, respectively, and placed into the Teflon-liner at an angle against the wall. Then 0.32 ml of $Ti(OCH_2CH_2CH_2CH_3)_4$ was slowly added into the HCl solution within 5 min and transferred into the Teflon-lined stainless steel autoclave (50 ml) for $TiO_2$NR growing at 150°C for 12 h. For the electrophoretic deposition of HGNs on the $TiO_2$NR anode (figure 1*b*), a two-electrode system was used with the Pt foil as the cathode and the separation distance of two electrodes was 15 mm. A DC voltage of 35 V was applied for 3–13 min to infuse the HGNs on the $TiO_2$NR surface in a 10 ml of HGN dispersion solution (0.04 mM) while ceaselessly stirred. Then the electrodes were dried at 60°C to improve the contact between HGNs and $TiO_2$NR. The $TiO_2$NR/HGN samples were further sensitized *in situ* with CdS by SILAR deposition by immersing in 0.1 mol $l^{-1}$ $Cd(NO_3)_2$ ethanol solution and 0.1 mol $l^{-1}$ $Na_2S$ methanol : D.I. water solution (1 : 1 by volume) several times. Various quantities of HGNs and CdS were easily controlled by changing the deposition time of HGNs and SILAR cycles for CdS to optimize the photovoltaic performance of photoanodes. In addition, the FTO/$TiO_2$NR/CdS photoanode without HGNs and the FTO/$TiO_2$NR/SGN/CdS photoanode were also prepared as control to explore the effect of HGNs in the photoelectrochemical behaviours of photoanodes.

## 2.4. Characterization

The morphologies of different samples were characterized by transmission electron microscopy (TEM, Philips CM 300 FEG) at 200 kV, and scanning electron microscopy (SEM, Hitachi S4800, Japan) with an energy-dispersive X-ray (EDX) spectrometer. X-ray diffraction (XRD) pattern of sample was determined by a diffractometer (Bruker AXS D8) with Cu Kα radiation ($\lambda = 0.15418$ nm) at an accelerating voltage of 40 kV and applied current of 40 mA. The extinction spectra of samples were measured by the UV–vis spectrophotometer (Hitachi U3900).

Photoelectrochemical performances of samples were performed on a CHI 630D electrochemical system (Chenhua Instruments, Shanghai, China). The system consisted of three electrodes and a transparent quartz cell, which was filled with $Na_2S$ (0.2 mol $l^{-1}$) and $Na_2SO_3$ (0.2 mol $l^{-1}$) electrolyte (25 ml). A Pt foil was used as a counter electrode with Ag/AgCl/KCl as a reference electrode. All the samples (10 mm × 20 mm) with impregnated area of 1.5 $cm^2$ were employed as working electrodes. The curves of photovoltage and photocurrent versus times were recorded by the electrochemical system using a 150 W Xe lamp (filtered, $\lambda \geq 300$ nm) as the light source. The illumination intensity near the sample surface was about 100 mW $cm^{-2}$. Incident photon conversion efficiency (IPCE) was measured on an IPCE measurement system (Solar Cell Scan 100, Zolix) with a 150 W Xe lamp aligned into a monchromator scanning. All measurements were carried out in ambient air and at room temperature without encapsulation.

# 3. Results and discussion

## 3.1. Microstructures of $TiO_2$NR/HGN/CdS photoanode

The TEM image of concentrated HGNs is shown in figure 2*a*. The strong contrast difference with a bright centre and a much darker edge confirms their hollow architecture, and their average outer diameter and inner one are about $33 \pm 2.7$ nm and $19 \pm 2.3$ nm, respectively, as observed from the size distribution histograms (figure 2*b*). Figure 2*c* displays the SPR absorption band centred at 575 nm, which corresponds to HGNs [35,39,40]. The XRD pattern of the as-prepared HGNs on the glass substrate (figure 2*d*) shows four diffraction peaks at ($2\theta$) 38.0°, 44.2°, 64.6° and 77.8°, respectively, which correspond to (111), (200), (220) and (311) crystallographic planes [41], confirming the face-centred cubic gold (JCPDS, 04-0784).

The SEM micrograph in figure 3*a* presents well-aligned $TiO_2$NRs uniformly grown on the FTO substrates. The cross-sectional SEM image of $TiO_2$NR with HGNs decorated in figure 3*b* indicates that the length of $TiO_2$NR is about 1.75 µm. The HGNs distributed on the $TiO_2$NRs surface are brighter than $TiO_2$ (figure 3*b*,*c*). From the cross-sectional and surface SEM images of $TiO_2$NR/HGN/CdS sample, we can see that many CdS QDs are well adsorbed onto the side walls of $TiO_2$NR/HGN via SILAR. The EDS result shows the existence of $TiO_2$, CdS and gold (figure 3*f*). The XRD peaks at ($2\theta$) 36.0° and 62.7° (figure 4*a*) correspond to (101) and (002) planes of rutile structure of $TiO_2$ [42] (JCPDS, 21-1276), respectively. The XRD peaks at ($2\theta$) 26.6° and 43.7° are assigned to the (111) and (220) planes of cubic CdS structure (JCPDS, 65-2887) in figure 4*b*,*c*. The crystallographic peaks of HGNs are indistinguishable in $TiO_2$NR/HGN/CdS sample due to the low content of HGNs (figure 3*d*). Furthermore, the TEM and high-resolution TEM images for $TiO_2$NR/HGN and $TiO_2$NR/HGN/CdS were also recorded (figure 5). The (111) facet of gold (lattice fringe spacing of 0.236 nm) and (101) facet of $TiO_2$NR (lattice fringe spacing of 0.314 nm) are easily distinguished from the high-resolution TEM image (figure 5*b*), and the (111) crystal face of CdS with the lattice fringe spacing of 0.336 nm is also shown in figure 5*d*.

## 3.2. Photovoltaic performance of $TiO_2$NR/HGN/CdS photoanode

Figure 6 displays the UV–vis absorption spectra of different photoanodes. The absorption of bare $TiO_2$NR is featureless above 380 nm, but $TiO_2$NR/HGN shows an obvious absorption in the visible region between 550 and 700 nm with respect to $TiO_2$NR, which is attributed to the plasmon resonance absorption peak arising from HGNs [35,43]. As compared to the HGNs colloid in D.I. water (figure 2*c*), the plasmon band of HGNs for $TiO_2$NR/HGN is red-shifted and broadened owing to the high refractive index of rutile $TiO_2$ (2.55–2.76) surrounding HGNs. Since the plasmon resonance frequency of HGNs is sensitively dependent on the surrounding matter, the local electromagnetic field enhancement around the HGNs might cause the red shift of absorption and increase light absorption of the surrounding photosensitizer [34]. This means that the optical feature of $TiO_2$NR/HGN is a synergistic effect between $TiO_2$NR and HGNs. The broad peak from 380 to 480 nm corresponds to the absorption of CdS QDs. Compared with $TiO_2$NR/CdS, there is a significant absorption enhancement of $TiO_2$NR/HGN/CdS photoanode in the region from 550 to 750 nm, which is attributed to the behaviour of HGNs. When considering the $TiO_2$NR/HGN and $TiO_2$NR/HGN/CdS photoanodes, the obvious red shift of the plasmon band of HGNs could be attributed to the HGNs-mediated near-field enhancement effect and near-field coupling with photosensitive semiconductor [34]. Mahmoud's study indicated that HGNs possessed stronger plasmonic electromagnetic field and wider plasmon resonant wavelengths than the special SGNs with same size via the finite difference time domain (FDTD) calculations, which hinted that the HGNs might be more suitable as the scatter centre to concentrate photons and enhance the light absorption when compared to the SGNs [44]. To explore the light-harvesting capabilities of HGNs, the optimum amount of the HGNs was found by varying the density of HGNs on the $TiO_2$NR surface with the electrophoretic deposition time from 3 to 13 min (the number of SILAR cycles applied to deposit CdS was 4). It can be seen that as the amount of HGNs in the photoanodes increases (from 0.6 to 3.3 wt% obtained from EDS results), the absorption of $TiO_2$NR/HGN/CdS in the visible region between 500 and 700 nm is intensified by the impact of SPR absorption peak arising from HGNs when the electrophoresis times of HGNs increases from 3 to 9 min (figure 7*a*), and tends to stabilize with the electrophoresis times rising up to 13 min. Besides, we observe a slight red shift in the optical absorption of $TiO_2$NR/HGN/CdS, which may be attributed to an increase in HGNs clusters at a certain high amounts [45].

Furthermore, the photocurrent and photovoltage of $TiO_2$NR/HGN/CdS photoanodes were examined by constructing a photoelectrochemical cell system with the Ag/AgCl/KCl as a reference electrode and platinum foil as a counter electrode in the $Na_2S/Na_2SO_3$ electrolyte (0.2 mol $l^{-1}$). The

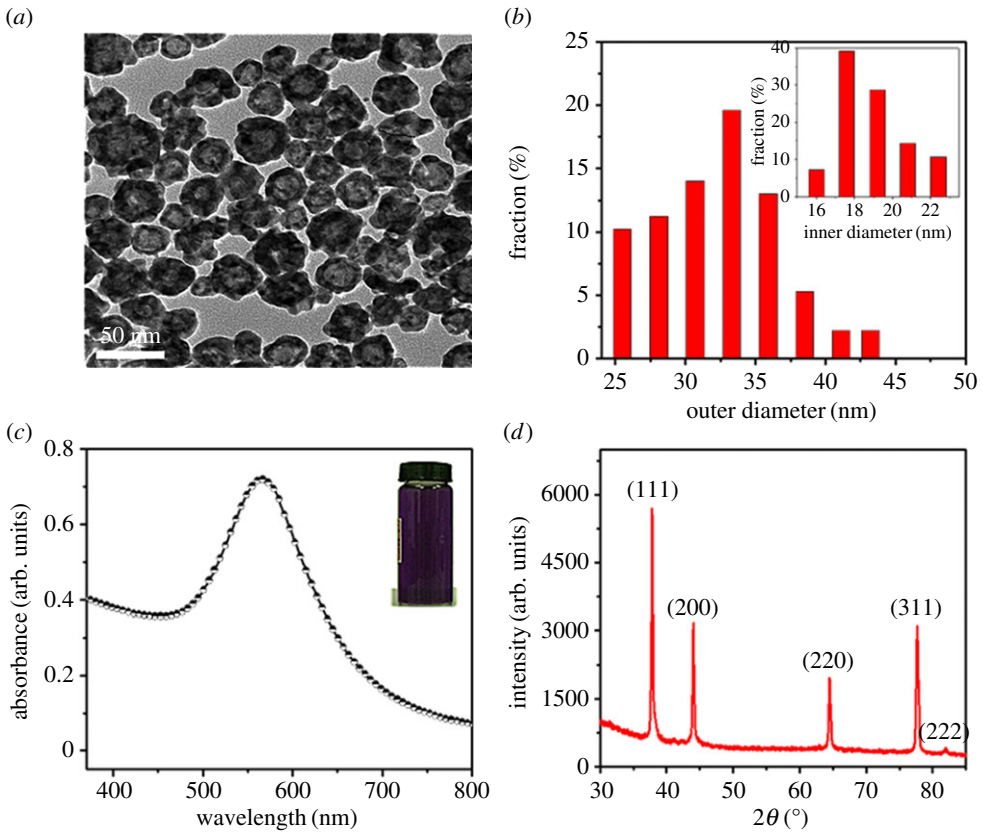


**Figure 2.** (*a*) TEM image, (*b*) size distribution histograms, (*c*) UV–vis absorption spectrum and (*d*) XRD spectrum of HGNs.

current densities in all samples are almost zero without photoillumination (figure 7*b*). Compared to $TiO_2$NR/CdS, the $TiO_2$NR/HGN/CdS samples show superior photoelectrochemical properties by introducing HGNs. The photocurrent responses of the $TiO_2$NR/HGN/CdS photoanodes are strongly dependent on the deposition time of HGNs, in which the photocurrent of $TiO_2$NR/HGN/CdS photoanode presents a first increased and then decreased tendency with the maximum obtained at the electrophoresis times of 7 min ($TiO_2$NR/HGN7/CdS with 2.7 wt% HGNs obtained from EDS result). The photovoltage also shows a similar variation trend with the maximum obtained for the $TiO_2$NR/HGN5/CdS or $TiO_2$NR/HGN7/CdS system (figure 7*c*). The schematic representation of separation and transfer of electron-hole pairs in CdS QD-sensitized $TiO_2$ solar cell with plasmonic HGNs is demonstrated in figure 1*b*. Upon photoillumination, CdS QDs will preferentially absorb incident light to produce photogenerated electron-hole pairs. The electrons are then injected into the conduction band of $TiO_2$NR and further rapidly transported to the FTO substrate, while the holes are got by the electrolyte, resulting in the photocurrent in the circuit and open-circuit voltage. When the plasmonic HGNs are introduced into the $TiO_2$NR/CdS system, the HGNs would absorb the incident light, scatter and trap it into the CdS film by multiple scattering, causing an increase of effective optical path length in the cell (figure 1*b*) [33,46]. This could favour the strong local-field enhancement around the HGNs and near-field coupling with the CdS semiconductor, increasing the absorption of CdS and the number of electron-hole pairs [27]. However, the intensity of localized electric field is weakened with the reduced 'hot spots' when the HGNs greatly overlap [33] (as the recombination centres of the electrons and holes), resulting in the dramatic drop in the photovoltaic response for the $TiO_2$NR/HGN9/CdS and $TiO_2$NR/HGN13/CdS systems. The IPCE result measured in the 300–600 nm wavelength range (figure 7*d*) follows a similar trend to that observed in the photocurrent responses spectra (figure 7*b*). The IPCE spectral characteristics correspond well to the absorbance spectra of the CdS-sensitized photoanodes. It can be observed that HGN-decorated $TiO_2$NR/CdS photoanodes show improved photoactivity from 380 to 530 nm compared with the $TiO_2$NR/CdS, especially in the visible region from 450 to 530 nm due to the main contribution from HGNs. These results demonstrate that excitation of the HGNs SPR is responsible for the improved photoelectrochemical properties of $TiO_2$NR/HGN/CdS structures. When using the SGNs with similar size to the HGNs, the photoelectrochemical properties of $TiO_2$NR/SGN/CdS structures are obviously

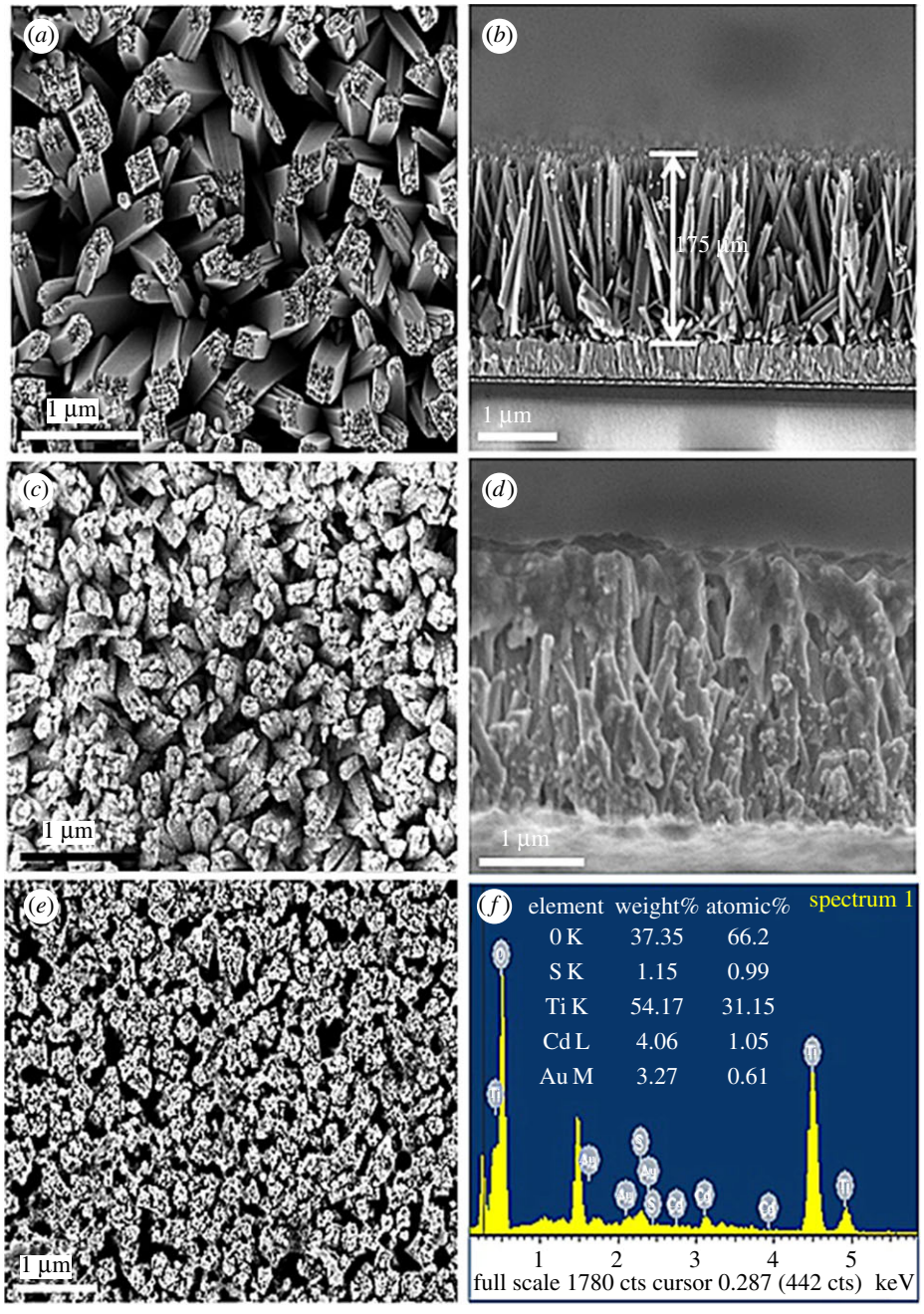


**Figure 3.** SEM images of (*a*) $TiO_2$NR, (*c*) $TiO_2$NR/HGN and (*e*) $TiO_2$NR/HGN/CdS hybrids. Cross-sectional SEM micrographs of (*b*) $TiO_2$NR/HGN and (*d*) $TiO_2$NR/HGN/CdS hybrids. The electrophoretic deposition time of HGNs was 7 min, and the number of SILAR cycles applied to deposit CdS was 7. (*f*) EDS result of $TiO_2$NR/HGN/CdS hybrid. The electrophoretic deposition time of HGNs was 9 min, and the number of SILAR cycles applied to deposit CdS was 7.

inferior to the $TiO_2$NR/HGN/CdS structures, demonstrating the preponderance of HGNs in light harvesting.

For further optimize the photovoltaic performance of $TiO_2$NR/HGN/CdS photoanode, the amount of CdS QDs was adjusted by changing the SILAR cycles. The UV–vis absorption spectra of $TiO_2$NR/HGN/CdS photoanodes are enhanced by increasing the number of SILAR cycles ($n = 2, 4, 6, 7$) (figure 8*a*). Furthermore, the absorbance spectra related to plasmon mode of HGNs in the range from 550 to 700 nm show a red shift with the increasing number of SILAR cycles, indicating the increased coupling and synergistic effect between HGNs and CdS. Additionally, the photocurrent density and open-circuit voltage increase with the number of SILAR cycles up to 4 (figure 8*b*,*c*). However, those parameters further

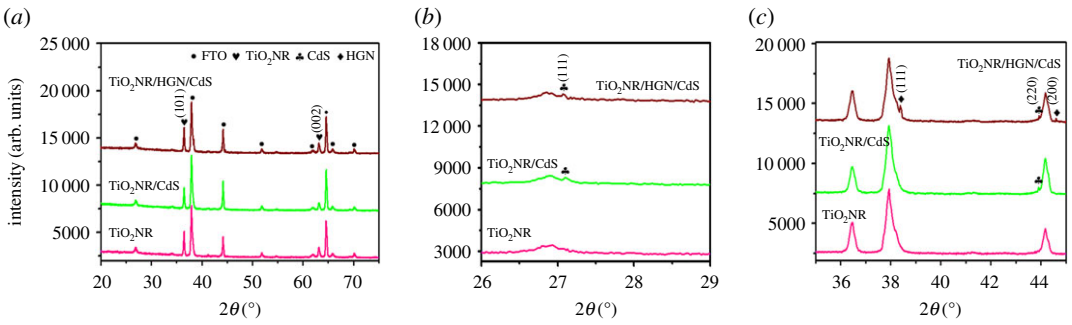


**Figure 4.** (*a*) XRD patterns of $TiO_2$NR, $TiO_2$NR/CdS and $TiO_2$NR/HGN/CdS. Detailed XRD patterns of these three samples in the range ($2\theta$) (*b*) from 26° to 29° and (*c*) from 36° to 45°. The electrophoretic deposition time of HGNs was 13 min, and the number of SILAR cycles applied to deposit CdS was 7.

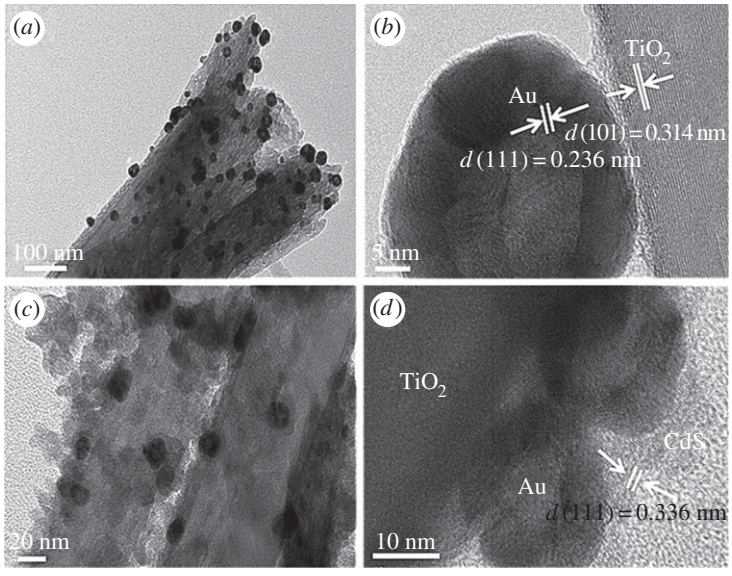


**Figure 5.** TEM images of (*a*) $TiO_2$NR/HGN and (*c*) $TiO_2$NR/HGN/CdS hybrids. High-resolution TEM images of (*b*) $TiO_2$NR/HGN and (*d*) $TiO_2$NR/HGN/CdS hybrids.

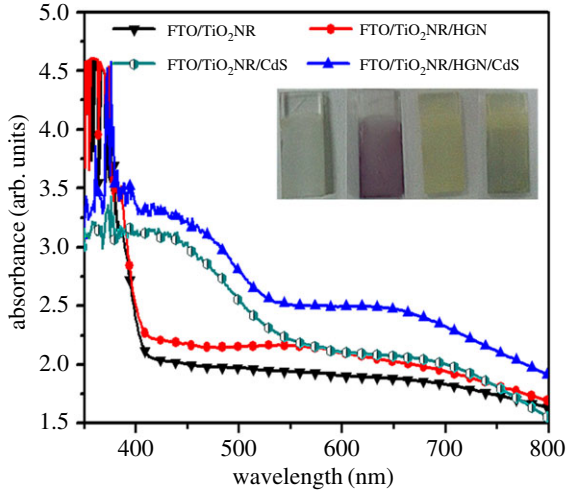


**Figure 6.** UV–vis absorption spectra and photographs of $TiO_2$NR, $TiO_2$NR/HGN, $TiO_2$NR/HGN/CdS and $TiO_2$NR/CdS hybrids. The electrophoretic deposition time of HGNs was 13 min, and the number of SILAR cycles applied to deposit CdS was 7.

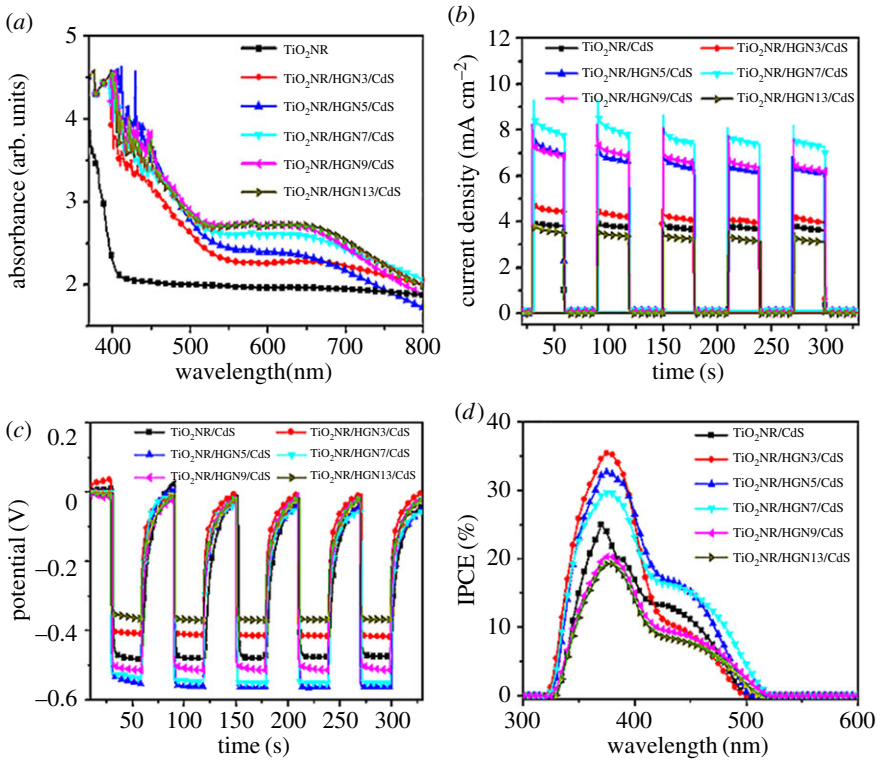


**Figure 7.** (*a*) UV–vis absorption spectra, (*b*) photocurrent density, (*c*) open-circuit voltage and (*d*) IPCE of $TiO_2$NR/HGN/CdS hybrids with varied amounts of HGNs conducted by varied electrophoretic deposition times. The number of SILAR cycles applied to deposit CdS was 4.

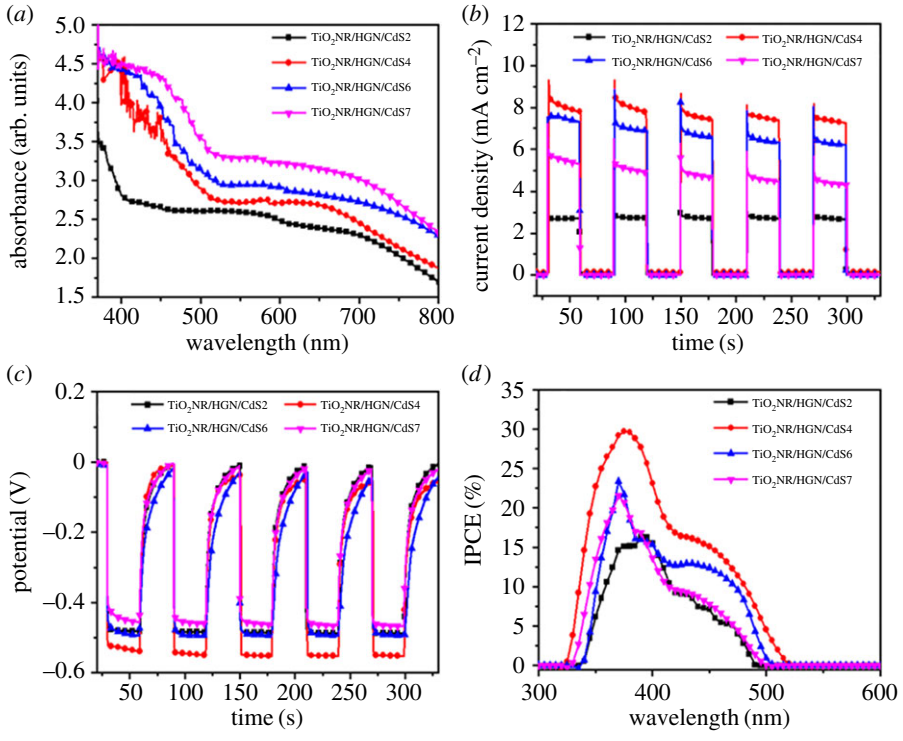


**Figure 8.** (*a*) UV–vis absorption spectra, (*b*) photocurrent density, (*c*) open-circuit voltage and (*d*) IPCE of $TiO_2$NR/HGN/CdS hybrids with different numbers of SILAR cycles applied to deposit CdS. The electrophoretic deposition time of HGNs was 7 min.

decrease when the number of SILAR cycles is up to 6 and 7. This phenomenon may be attributed to the following reasons: firstly, the excessive SILAR cycles would lead to the conglomeration of CdS QDs, resulting in the poor charge injection efficiency due to the large QDs; secondly, the aggregation of CdS QDs may form excessive grain boundaries between CdS NPs, which would act as potential barriers and enhance the recombination possibilities of electron-hole pairs, leading to a decrease in photovoltaic behaviours [34,47,48]; thirdly, the conglomeration of excess CdS crystal nucleus may hinder the diffusion of the electrolyte into the $TiO_2$NR/HGN/CdS photoanode, which also limits the efficiency of charge separation and charge extraction, as shown in the IPCE responses (figure 8*d*).

# 4. Conclusion

In summary, the 'sandwich'-structured $TiO_2$NR/HGN/CdS photoanode was fabricated by using plasmonic HGNs as light concentrators to effectively enhance photovoltaic performance. The light scattering and trapping of plasmonic HGNs and the near-field coupling of plasmonic HGNs with the photosensitive layers increase the absorption and the number of photoproduced electron-hole pairs of semiconductor. The $TiO_2$NR/HGN/CdS photoanode with optimized design presents an obvious predominance in the improvement of photovoltaic performances such as photocurrent, open-circuit voltage and incident photon-to-current conversion efficiency when compared to the $TiO_2$NR/CdS one. The plasmonic light-trapping concept would have potential applications in QDs-sensitized film solar cells and related energy conversion devices.

Data accessibility. The details of the research materials pertaining to this work have been provided in the manuscript itself.

Authors' contributions. H.D. and J.L. assisted the main experimental works to achieve the research results; H.W. and A.L. proposed the research and experiment; G.C. provided expertise suggestion. All authors gave final approval for publication.

Competing interests. We have no competing interests.

Funding. This work was supported by the National Natural Science Foundation of China (nos. 51572242, 11672269, 51375447 and 51475424), the Zhejiang Provincial Natural Science Foundation of China (no. LY16E020011), the Program for Innovative Research Team of Zhejiang Sci-Tech University (no. 15010039-Y) and the Opening Fund of State Key Laboratory of Nonlinear Mechanics.

Acknowledgement. We thank Peigang Li from Zhejiang Sci-Tech University for helpful discussions.

# References

1. O'Regan B, Gratzel M. 1991 A low-cost, high-efficiency solar cell based on dye-sensitized colloidal $TiO_2$ films. *Nature* **353**, 737–740. (doi:10.1038/353737a0)
2. Kamat PV, Tvrdy K, Baker DR, Radich JG. 2010 Beyond photovoltaics: semiconductor nanoarchitectures for liquid-junction solar cells. *Chem. Rev.* **110**, 6664–6688. (doi:10.1021/cr100243p)
3. Kim SK, Gopi CVVM, Rao SS, Punnoose D, Kim HJ. 2016 Highly efficient yttrium-doped ZnO nanorods for quantum dot-sensitized solar cells. *Appl. Surf. Sci.* **365**, 136–142. (doi:10.1016/j.apsusc.2016.01.043)
4. Ghaffari M, Cosar MB, Yavuz HI, Ozenbas M, Okyay AK. 2012 Effect of Au nano-particles on $TiO_2$ nanorod electrode in dye-sensitized solar cells. *Electrochim. Acta* **76**, 446–452. (doi:10.1016/j.electacta.2012.05.058)
5. Wang XD, Li ZD, Shi J, Yu YH. 2014 One-dimensional titanium dioxide nanomaterials: nanowires, nanorods, and nanobelts. *Chem. Rev.* **114**, 9346–9384. (doi:10.1021/cr400633s)
6. Jin BB, Wang YF, Wang XQ, Zeng JH. 2016 Pulsed voltage deposited lead selenide thin film as efficient counter electrode for quantum-dot-sensitized solar cells. *Appl. Surf. Sci.* **369**, 436–442. (doi:10.1016/j.apsusc.2016.02.095)
7. Zhou R, Zhang QF, Tian JJ, Myers D, Yin M, Cao GZ. 2013 Influence of cationic precursors on CdS quantum-dot-sensitized solar cell prepared by successive ionic layer adsorption and reaction. *J. Phys. Chem. C* **117**, 26 948–26 956. (doi:10.1021/jp410615b)
8. Narayanan R, Reddy BN, Deepa M. 2012 Facile charge propagation in CdS quantum dot cells. *J. Phys. Chem. C* **116**, 7189–7199. (doi:10.1021/jp211200f)
9. Lee HJ, Bang J, Park J, Kim SJ, Park SM. 2010 Multilayered semiconductor (CdS/CdSe/ZnS)-sensitized $TiO_2$ mesoporous solar cells: all prepared by successive ionic layer adsorption and reaction processes. *Chem. Mater.* **22**, 5636–5643. (doi:10.1021/cm102024s)
10. Hensel J, Wang GM, Li Y, Zhang JZ. 2010 Synergistic effect of CdSe quantum dot sensitization and nitrogen doping of $TiO_2$ nanostructures for photoelectrochemical solar hydrogen generation. *Nano Lett.* **10**, 478–483. (doi:10.1021/nl903217w)
11. Yochelis S, Hodes G. 2004 Nanocrystalline CdSe formation by direct reaction between Cd ions and selenosulfate solution. *Chem. Mater.* **16**, 2740–2744. (doi:10.1021/cm049895v)
12. Bang JH, Kamat PV. 2009 Quantum dot sensitized solar cells. A tale of two semiconductor nanocrystals: CdSe and CdTe. *ACS Nano* **3**, 1467–1476. (doi:10.1021/nn900324q)
13. Kramer IJ, Levina L, Debnath R, Zhitomirsky D, Sargent EH. 2011 Solar cells using quantum funnels. *Nano Lett.* **11**, 3701–3706. (doi:10.1021/nl201682h)
14. Santra PK, Kamat PV. 2013 Tandem-layered quantum dot solar cells: tuning the photovoltaic response with luminescent ternary cadmium chalcogenides. *J. Am. Chem. Soc.* **135**, 877–885. (doi:10.1021/ja310737m)
15. Choi YW, Seol M, Kim W, Yong KJ. 2014 Chemical bath deposition of stoichiometric CdSe quantum dots for efficient quantum-dot-sensitized solar cell application. *J. Phys. Chem. C* **118**, 5664–5670. (doi:10.1021/jp411221q)
16. Li ZX, Xie YL, Xu H, Wang TM, Xu ZG, Zhang HL. 2011 Expanding the photoresponse range of $TiO_2$ nanotube arrays by CdS/CdSe/ZnS quantum dots co-modification. *J. Photoch. Photobio. A* **224**, 25–30. (doi:10.1016/j.jphotochem.2011.09.002)
17. Kou HR, Li XF, Shan H, Fan LL, Yan B, Li DJ. 2017 An optimized $Al_2O_3$ layer for enhancing the anode performance of $NiCo_2O_4$ nanosheets for sodium-ion batteries. *J. Mater. Chem. A*, **5**, 17 881–17 888. (doi:10.1039/C7TA01870C)
18. Li XJ *et al.* 2017 Rational design of $Sn/SnO_2$/porous carbon nanocomposites as anode materials for

sodium-ion batteries. *Appl. Sur. Sci.* **412**, 170–176. (doi:10.1016/j.apsusc.2017.03.203)

19. Wu HP, Yang Z, Cao BB, Zhang Z, Zhu K, Wu BB, Jiang SF, Chai GZ. 2017 Wetting and dewetting transitions on submerged superhydrophobic surfaces with hierarchical structures. *Langmuir* **33**, 407–416. (doi:10.1021/acs.langmuir.6b03752)
20. Wu HP, Zhu K, Cao BB, Zhang Z, Wu BB, Liang LH, Chai GZ, Liu AP. 2017 Smart design of wettability-patterned gradients on substrate-independent coated surfaces to control unidirectional spreading of droplets. *Soft Matter.* **13**, 2995. (doi: 10.1039/C6SM02864K)
21. Tan DP, Ni YS, Zhang LB. 2017 Two-phase sink vortex suction mechanism and penetration dynamic characteristics in ladle teeming process. *J. Iron Steel Res. Int.* **24**, 669–677. (doi:10.1016/S1006-706X(17)30101-2)
22. Tan DP, Zhang LB, Ai QL. 2016 An embedded self-adapting network service framework for networked manufacturing system. *Int. J. Adv. Manuf. Tech.* **85**, 1261–1274. (doi:10.1007/s00170-015-8044-8)
23. Yang ZS, Chen CY, Liu CW, Li CL, Chang HT. 2011 Quantum dot–sensitized solar cells featuring CuS/CoS electrodes provide 4.1% efficiency. *Adv. Energy Mater.* **1**, 259–264. (doi:10.1002/aenm.201000029)
24. Lee YL, Chang CH. 2008 Efficient polysulfide electrolyte for CdS quantum dot-sensitized solar cells. *J. Power Sources* **185**, 584–588. (doi:10.1016/j.jpowsour.2008.07.014)
25. Jiang RB, Li BX, Fang CH, Wang JF. 2014 Metal/semiconductor hybrid nanostructures for plasmon-enhanced applications. *Adv. Mater.* **26**, 5274–5309. (doi:10.1002/adma.201400203)
26. Kochuveedu ST, Jang YH, Kim DH. 2013 A study on the mechanism for the interaction of light with noble metal-metal oxide semiconductor nanostructures for various photophysical applications. *Chem. Soc. Rev.* **42**, 8467–8493. (doi:10.1039/c3cs60043b)
27. Atwater HA, Polman A. 2010 Plasmonics for improved photovoltaic devices. *Nat. Mater.* **9**, 205–213. (doi:10.1038/nmat2629)
28. Wang Q, Butburee T, Wu X, Chen HJ, Liu G, Wang LZ. 2013 Enhanced performance of dye-sensitized solar cells by doping Au nanoparticles into photoanodes: a size effect study. *J. Mater. Chem. A* **1**, 13 524–13 531. (doi:10.1039/c3ta12692g)
29. Chander N, Khan AF, Thouti E, Sardana SK, Chandrasekhar PS, Dutta V, Komarala VK. 2014 Size and concentration effects of gold nanoparticles on optical and electrical properties of plasmonic dye sensitized solar cells. *Sol. Energy* **109**, 11–23. (doi:10.1016/j.solener.2014.08.011)
30. Xiao FX. 2012 Layer-by-layer self-assembly construction of highly ordered metal-$TiO_2$ nanotube arrays heterostructures (M/TNTs, M = Au, Ag, Pt) with tunable catalytic activities. *J. Phys. Chem. C* **116**, 16 487–16 498. (doi:10.1021/jp3034984)
31. Zarazua I, De La Rosa E, Lopez-Luke T, Reyes-Gomez J, Ruiz S, Chavez CA, Zhang JZ. 2011 Photovoltaic conversion enhancement of CdSe quantum dot-sensitized $TiO_2$ decorated with Au nanoparticles and P3OT. *J. Phys. Chem. C* **115**, 23 209–23 220. (doi:10.1021/jp207744n)
32. Zarick HF, Hurd O, Webb JA, Hungerford C, Erwin WR, Bardhan R. 2014 Enhanced efficiency in dye-sensitized solar cells with shape-controlled plasmonic nanostructures. *ACS Photonics* **1**, 806–811. (doi:10.1021/ph500281v)
33. Liu AP, Ren QH, Yuan M, Xu T, Tan ML, Zhao TY, Dong WJ, Tang WH. 2013 Layer-by-layer assembled porous CdSe films incorporated with plasmonic gold and improved photoelectrochemical behaviors. *Electrochim. Acta* **108**, 680–689. (doi:10.1016/j.electacta.2013.07.019)
34. Liu AP, Ren QH, Zhao M, Xu T, Yuan M, Zhao TY, Tang WH. 2014 Photovoltaic performance enhancement of CdS quantum dot-sensitized $TiO_2$ photoanodes with plasmonic gold nanoparticles. *J. Alloy. Compd.* **589**, 218–225. (doi:10.1016/j.jallcom.2013.11.106)
35. Lu B, Liu AP, Wu HP, Shen QP, Zhao TY, Wang JS. 2016 Hollow Au-$Cu_2O$ core-shell nanoparticles with geometry-dependent optical properties as efficient plasmonic photocatalysts under visible light. *Langmuir* **32**, 3085–3094. (doi:10.1021/acs.langmuir.6b00331)
36. Gong X, Tang J, Ji YX, Wu BB, Wu HP, Liu AP. 2015 Adjustable plasmonic optical properties of hollow gold nanospheres monolayers and LSPR-dependent surface-enhanced Raman scattering of hollow gold nanosphere/graphene oxide hybrids. *RSC Adv.* **5**, 42 653–42 662. (doi:10.1039/c5ra08057f)
37. Liang HP, Wan LJ, Bai CL, Jiang L. 2005 Gold hollow nanospheres: tunable surface plasmon resonance controlled by interior-cavity sizes. *J. Phys. Chem. B* **109**, 7795–7800. (doi:10.1021/jp045006f)
38. Chandra M, Dowgiallo AM, Knappenberger KL. 2010 Controlled plasmon resonance properties of hollow gold nanosphere aggregates. *J. Am. Chem. Soc.* **132**, 15 782–15 789. (doi:10.1021/ja106910x)
39. Schwartzberg AM, Olson TY, Talley CE, Zhang JZ. 2016 Synthesis, characterization, and tunable optical properties of hollow gold nanospheres. *J. Phys. Chem. B* **110**, 19 935–19 944. (doi:10.1021/jp062136a)
40. Huang J, Kim KH, Choi N, Chon H, Lee S, Choo J. 2011 Preparation of silica-encapsulated hollow gold nanosphere tags using layer-by-layer method for multiplex surface-enhanced Raman scattering detection. *Langmuir* **27**, 10 228–10 233. (doi:10.1021/la201739n)
41. He H, Cai WP, Lin YX, Chen BS. 2010 Au nanochain-built 3D netlike porous films based on laser ablation in water and electrophoretic deposition. *Chem. Commun.* **46**, 7223–7225. (doi:10.1039/c0cc00504e)
42. Liu B, Aydil ES. 2009 Growth of oriented single-crystalline rutile $TiO_2$ nanorods on transparent conducting substrates for dye-sensitized solar cells. *J. Am. Chem. Soc.* **131**, 3985–3990. (doi:10.1021/ja8078972)
43. Lim SP, Pandikumar A, Huang NM, Lim HN. 2015 Facile synthesis of Au@$TiO_2$ nanocomposite and its application as a photoanode in dye-sensitized solar cells. *RSC Adv.* **5**, 44 398–44 407. (doi:10.1039/c5ra06220a)
44. Mahmoud MA, El-Sayed MA. 2013 Substrate effect on the plasmonic sensing ability of hollow nanoparticles of different shapes. *J. Phys. Chem. B* **117**, 4468–4477. (doi:10.1021/jp3085793)
45. Li Y, Wang H, Feng QY, Zhou G, Wang ZS. 2013 Gold nanoparticles inlaid $TiO_2$ photoanodes: a superior candidate for high-efficiency dye-sensitized solar cells. *Energy Environ. Sci.* **6**, 2156–2165. (doi:10.1039/c3ee23971c)
46. Li JT, Cushing SK, Zheng P, Senty T, Meng FK, Bristow AD, Manivannan A, Wu NQ. 2014 Solar hydrogen generation by a CdS-Au-$TiO_2$ sandwich nanorod array enhanced with Au nanoparticle as electron relay and plasmonic photosensitizer. *J. Am. Chem. Soc.* **136**, 8438–8449. (doi:10.1021/ja503508g)
47. Hao EC, Yang B, Zhang JH, Zhang X, Sun JQ, Shen SC. 1998 Assembly of alternating $TiO_2$/CdS nanoparticle composite films. *J. Mater. Chem.* **8**, 1327–1328. (doi:10.1039/a802655f)
48. Nozik AJ, Beard MC, Luther JM, Law M, Ellingson RJ, Johnson JC. 2010 Semiconductor quantum dots and quantum dot arrays and applications of multiple exciton generation to third-generation photovoltaic solar cells. *Chem. Rev.* **110**, 6873–6890. (doi:10.1021/cr900289f)